



FERMILAB-Pub-83/108-EXP
7420.616
(Submitted to Zeit. Phys. C)

NUCLEON STRUCTURE FUNCTIONS FROM HIGH ENERGY NEUTRINO INTERACTIONS WITH IRON AND QCD RESULTS

D. MacFarlane, M. V. Purohit, R. L. Messner, and D. B. Novikoff
California Institute of Technology, Pasadena, California 91125

R. E. Blair, F. J. Sciulli, and M. H. Shaevitz
Columbia University, New York, New York 10027

H. E. Fisk, Y. Fukushima, B. Jin, Q. A. Kerns, T. Kondo,
P. A. Rapidis, S. L. Segler, R. J. Stefanski, D. Theriot, and D. Yovanovitch
Fermi National Accelerator Laboratory, Batavia, Illinois 60510

A. Bodek, R. N. Coleman, and W. L. Marsh
University of Rochester, Rochester, New York 14627

O. D. Fackler and K. A. Jenkins
Rockefeller University, New York, New York 10021

December 1983

Nucleon Structure Functions from High Energy Neutrino
Interactions With Iron and QCD Results

D.B. MacFarlane¹, M.V. Purohit²,
R.L. Messner³, D.B. Novikoff⁴
California Institute of Technology, Pasadena, CA 91125

R.E. Blair, F.J. Sciulli, M.H. Shaevitz
Columbia University, New York, NY 10027

H.E. Fisk, Y. Fukushima⁵, B.N. Jin⁶, Q.A. Kerns
T. Kondo⁵, P.A. Rapidis, S.L. Segler,
R.J. Stefanski, D. Theriot, D.D. Yovanovitch
Fermilab, Batavia, IL 60510

A. Bodek, R.N. Coleman², W.L. Marsh²
University of Rochester, Rochester, NY 14627

O.D. Fackler, K.A. Jenkins⁷
Rockefeller University, New York, NY 10021

-
1. Now at the University of Toronto, Toronto, Ontario M5S 1A7, Canada.
 2. Now at Fermilab, P.O. Box 500, Batavia, IL 60510, USA.
 3. Now at SLAC, Stanford, CA 94305, USA.
 4. Now at Hughes Aircraft Co., El Segundo, CA 90245, USA.
 5. Now at the National Laboratory for High Energy Physics, Tsukuba-gun, Ibaraki-ken 305, Japan.
 6. Now at the Institute for High Energy Physics, Peking, P.R. China.
 7. Now at the IBM Thomas J. Watson Research Center, P.O. Box 218, Yorktown Heights, NY 10598, USA.

1 Experiment

We report results for the structure functions $F_2(x, Q^2)$ and $xF_3(x, Q^2)$ obtained from a high statistics sample of neutrino and anti-neutrino charged current events. The data were taken using the Lab E detector in the dichromatic (narrow-band) neutrino beam at Fermilab. A total of 150000 neutrino and 23000 anti-neutrino charged current events were obtained in the experiment E616 at five momentum settings of the secondary beam: 120, 140, 168, 200 and 250 GeV/c.

Use of the dichromatic beam as the neutrino source allows a calculation of neutrino flux to be made from measured properties of the secondary hadron beam. This technique minimizes the overall systematic errors on both the total cross section [1] and structure function results. The dichromatic beam [2] consists of electrons, pions, kaons and protons produced by the interaction of 400 GeV/c primary protons with a BeO target; the particles are sign and momentum-selected by a point to parallel magnetic channel ($\Delta p/p = 9.4\%$). The well collimated ($\sigma_\theta = 0.2\text{mr}$) secondary beam is then passed through an evacuated decay pipe where neutrinos are obtained from the weak decay of pions and kaons. A 910m shield of earth and steel ranges-out the decay muons, leaving only neutrinos at Lab E.

The total flux of secondaries in the decay pipe was monitored using ionization chambers [3]. These chambers have been calibrated using several different techniques. The estimated uncertainty in the absolute calibration is 2.5%. There is a further uncorrelated 1.6% and 4.2% error for neutrinos and anti-neutrinos respectively in applying the calibration measurement to conditions during data taking.

Secondary beam composition was determined using a Helium filled Čerenkov counter [3,4]. The fraction of pions, kaons and protons in the beam was determined by measuring the integrated Čerenkov light at a fixed angle to the beam as a function of counter pressure. The gas constant for the Čerenkov counter was measured using 200 GeV/c primary protons. Small corrections were made for backgrounds due to Čerenkov light from particles produced by interactions of the secondary beam with material upstream of the counter, and due to light scattering from dust on mirrors in the optical path. In addition, the analysis included the fact that a finite length radiator produces light within a diffractive envelope about the normal Čerenkov angle [4]. The counter response functions were predicted using a Monte Carlo calculation, and particle fractions were evaluated by fitting these functions to observed pressure curves. The estimated uncertainty in the determination of particle fractions is 1-4% for pions and 4-7% for kaons.

Beam direction and dispersion were measured using segmented ion chambers (SWICs). The mean direction of the secondary beam was maintained fixed to within a projected centroid of $\pm 3.0\text{cm}$ at Lab E, on a pulse by pulse basis. From the Čerenkov counter pressure curves mean momenta for kaons and protons were determined, a measurement redundant with the observed mean energy of neutrino events in the Lab E apparatus. The consistency of these

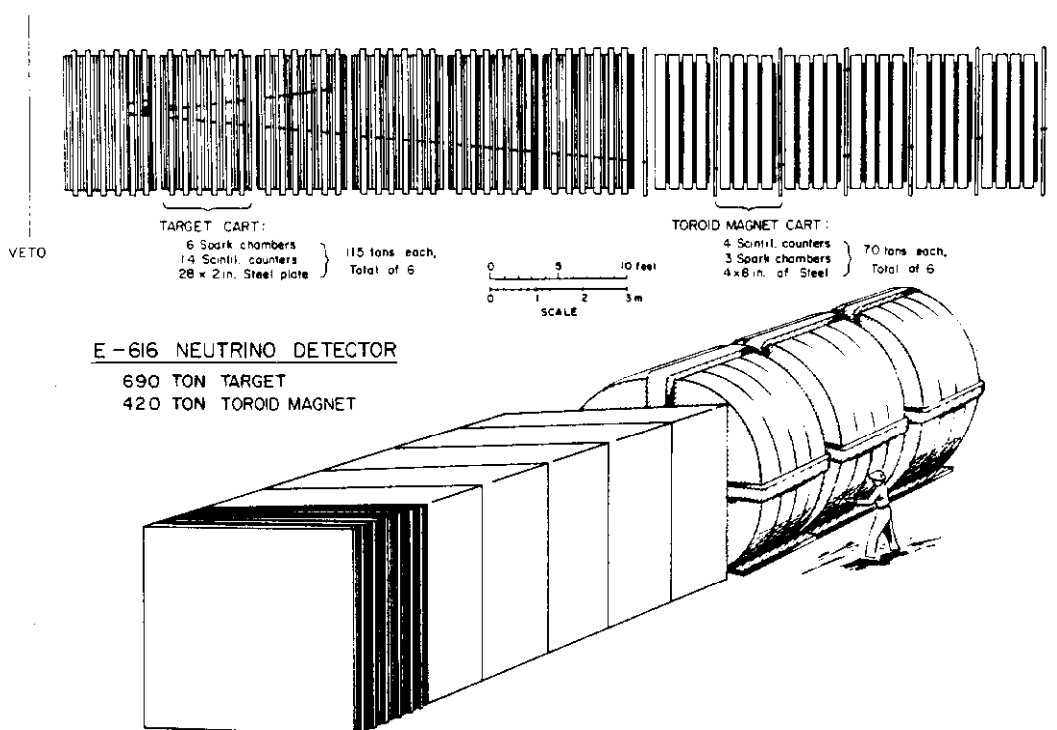


Figure 1 The Lab E detector.

measurements indicates a systematic error in mean secondary momentum of less than 1.5%. Corrections to the neutrino flux were also made for neutrinos from decays before the momentum defining collimator (wide band background); this flux was measured by taking data with the collimator closed.

The Lab E detector [5,6,7] (figure 1) consists of a calorimetric target of 640 tons of 3m square steel plates, interspersed with spark chambers (every 20cm of steel) and liquid scintillation counters (every 10cm of steel). This is followed by a steel toroidal spectrometer, 3.5m in diameter, also instrumented with spark chambers (every 80cm of steel) and scintillation counters (every 20cm of steel). Measurements of hadronic energy and the outgoing muon angle are made in the target, and the muon momentum was determined by the spectrometer. The rms resolutions for these measurements are:

$$\begin{aligned}\Delta E_H \text{ (GeV)} &= 0.93 + 0.78\sqrt{E_H \text{ (GeV)}} \\ \Delta E_\mu &= 0.11 E_\mu \\ \Delta \theta_\mu \text{ (mr)} &= 106/E_\mu \text{ (GeV)}\end{aligned}$$

where E_H and E_μ are the final state hadron and muon energies respectively, and θ_μ is the outgoing muon angle.

2 Analysis

Two types of triggers were used to obtain data for the structure function measurement. The muon trigger required a secondary muon originating in the target region and penetrating through 1/3 of the spectrometer. No hadron energy requirement was made, but the acceptance of the spectrometer limited the kinematic coverage of the trigger to those muons with angle $\theta_\mu < 250\text{mr}$. The penetration trigger demanded a minimum hadron energy of 4GeV in the target calorimeter, as well as a muon penetration of more than 160cm in steel. Except for a common front veto counter requirement, the logic of the two triggers was independent. Both triggers are satisfied over a large kinematic region and the trigger efficiencies are determined to be $99.5 \pm 0.5\%$ in the overlap region. Corrections of between 1% and 3% are made to compensate for the removal of events with poor fits to the muon track in the toroids.

Fiducial and kinematic cuts are applied to this data sample. Events due to neutrinos from pion decay are restricted to a region within a 76.2cm radius of the beam center. Those events induced by kaon decay neutrinos are included within a 254cm square, centered on the beam. Events are also confined to a longitudinal section of the target where hadron showers are fully contained within the target. Separation of events induced by neutrinos from pion and kaon decay, respectively, is extremely good [1].

Inclusive charged current events are usually parameterized by the quantities $y = E_H/E_\nu$, $Q^2 = 2E_\nu E_\mu(1 - \cos\theta_\mu)$ and $x = Q^2/2ME_H$. Kinematic cuts ensure good acceptance for events remaining after selection. These cuts are $E_\mu > 4\text{GeV}$ and $\theta_\mu < 200\text{mr}$, well within the limits of acceptance for penetration and muon events respectively. A further cut on the hadron energy ($E_H > 10\text{GeV}$) eliminates part of the lower Q^2 region where the x resolution is poor. The final data set after these cuts includes 65000 neutrino and 7000 anti-neutrino events.

The neutrino and anti-neutrino cross section in the standard (V-A) theory can be written in terms of structure functions (apart from small correction terms):

$$\frac{d^2\sigma^{\nu(\bar{\nu})}}{dx dy} = \frac{G^2 ME}{\pi} \left\{ \left(1 - y - \frac{Mxy}{2E} + \frac{y^2}{2} \frac{1 + 4M^2 x^2/Q^2}{1 + R(x, Q^2)} \right) F_2(x, Q^2) \pm \left(y - \frac{y^2}{2} \right) x F_3(x, Q^2) \right\} \quad (1)$$

For an isoscalar target:

$$\begin{aligned} 2xF_1(x, Q^2) &= q(x, Q^2) + \bar{q}(x, Q^2) \\ F_2(x, Q^2) &= 2xF_1(x, Q^2)(1 + R(x, Q^2))/(1 + 4M^2 x^2/Q^2) \\ xF_3(x, Q^2) &= q(x, Q^2) - \bar{q}(x, Q^2) \end{aligned} \quad (2)$$

where $q = u + d + s + c$ and $\bar{q} = \bar{u} + \bar{d} + \bar{s} + \bar{c}$ are respectively the quark and anti-quark momentum densities within the nucleon. In another notation, the structure functions

described above are the average of neutrino and antineutrino structure functions of the nucleon. No measurement of R is reported here; the structure functions are extracted under various assumptions about R which are consistent with present experimental measurements [8]. The propagator term for charged currents, with boson mass $M_W = 80\text{GeV}$, is not shown in (1), but is included in all of the analysis described here.

From the form of the differential cross section (1) it can be seen that the number of neutrino or anti-neutrino events in a given x and $\log Q^2$ bin is a linear combination of F_2 and xF_3 :

$$\begin{aligned} n_\nu/c_\nu &= a_\nu F_2(x, Q^2) + b_\nu xF_3(x, Q^2) \\ n_{\bar{\nu}}/c_{\bar{\nu}} &= a_{\bar{\nu}} F_2(x, Q^2) - b_{\bar{\nu}} xF_3(x, Q^2) \end{aligned} \quad (3)$$

The coefficients $a_{\nu(\bar{\nu})}$ and $b_{\nu(\bar{\nu})}$ are numerically evaluated integrals of products of flux and y -distribution factors. Various corrections need to be applied and are contained in $c_{\nu(\bar{\nu})}$. These include: (1) correction for the slightly non-isoscalar iron and scintillator target with a 6.5% excess of neutrons over protons, (2) strange sea correction, since the strange and charm components of the nucleon are not equal, (3) radiative corrections, following the prescription of de Rújula et al [9] and (4) bin center corrections. For the strange sea correction it was assumed that the charm component was zero and that the strange component of the sea was half the u (or d) component of the sea (1/2 SU(3) symmetric) [10,11]. The sea was obtained from fits to our structure function results. The suppression of transitions of d and s quarks to c was accounted for using slow-rescaling [21] with a charm mass of 1.5GeV. Corrections for acceptance are made by either weighting each event, or by including acceptance in the calculation of $a_{\nu(\bar{\nu})}$ and $b_{\nu(\bar{\nu})}$. Both approaches have been used with consistent results. Weights and acceptance are calculated in a model independent fashion by taking advantage of the symmetry of the cross section (1) with respect to rotations about the beam axis. Finally, the effect of resolution smearing is removed by correcting the observed number of events, $n_{\nu(\bar{\nu})}$, by a Monte Carlo determined correction factor.

Total cross sections from this experiment have been reported earlier and average about 10% higher [1] than some previous results. Therefore, the integrals of structure functions at fixed E_ν or Q^2 are also higher. Assuming simple scaling, it is possible to obtain the integrals of F_2 and xF_3 from the ν and $\bar{\nu}$ cross-section slopes determined by various experiments. The actual integrals may differ from these values due to experimentally observed levels of scale breaking which should be less than $\sim 3\%$. Table 1 is a comparison of integrals obtained from the cross sections and those we obtained by integrating the structure functions reported by the same experiments. Our results are quoted for two values of R to facilitate the comparisons. The integrals from the two techniques are in good agreement except for those from CDHS and the integral of F_2 from HPWF. The table implies then that the difference in integrals of structure functions reported by us and CDHS is only partly explained by total cross-section differences.

	CCFRR	CCFRR	CDHS	CHARM	HPWF
Reference	1, This expt.	1, This expt.	11,12	13,14	15
σ_ν/E	$.669 \pm .024$	$.669 \pm .024$	$.62 \pm .022$	$.604 \pm .032$	$.63 \pm .02$
$\sigma_{\bar{\nu}}/E$	$.340 \pm .020$	$.340 \pm .020$	$.30 \pm .013$	$.301 \pm .018$	$.30 \pm .01$
R	0.	0.1	0.1	0.	0.
$\int F_2$ predicted from cross-sections	$.466 \pm .015$	$.478 \pm .015$	$.436 \pm .012$	$.418 \pm .017$	$.430 \pm .010$
$\int xF_3$ predicted from cross-sections	$.312 \pm .030$	$.312 \pm .030$	$.303 \pm .024$	$.287 \pm .035$	$.313 \pm .021$
$\int F_2$ from data (statistical errors only)	$.474 \pm .003$	$.482 \pm .003$	$.402 \pm .002$	$.412 \pm .006$	$.458 \pm .003$
$\int xF_3$ from data (statistical errors only)	$.328 \pm .005$	$.326 \pm .005$	$.273 \pm .003$	$.285 \pm .012$	$.322 \pm .005$

Table 1

Integrals of structure functions compared with the same integrals obtained from cross-sections. In all cases the same assumptions are made about the strange sea (1/2 SU(3) symmetric), slow rescaling and the W-boson propagator. Some of the structure functions are extrapolated to cover the entire x -region. All these effects, along with scale breaking, do not change the results above by more than $\sim 3\%$.

F_2 and xF_3 are extracted with the constraint that the integrals of structure functions in overlapping x and Q^2 regions at different energy settings of the secondary beam be the same. This procedure removes most of the uncertainty induced by the errors on particle fractions in the decay pipe. The required adjustments to the ν and $\bar{\nu}$ fluxes are consistent with the expected errors on particle fractions from the Čerenkov analysis and are in excellent agreement with a cross-section rising linearly with energy. Table 2 lists our measurements of the total cross-section slopes before and after this procedure.

E_ν (GeV)	σ_ν/E Before corr.	σ_ν/E After corr.		$E_{\bar{\nu}}$ (GeV)	$\sigma_{\bar{\nu}}/E$ Before corr.	$\sigma_{\bar{\nu}}/E$ After corr.
37.1	.654±.012±.019	.691		36.9	.361±.010±.015	.340
44.7	.621±.010±.020	.664		45.0	.352±.007±.013	.331
54.0	.661±.008±.018	.696		54.0	.350±.007±.013	.342
63.5	.664±.010±.024	.695		63.8	.332±.009±.014	.344
75.4	.664±.008±.028	.686		75.6	.331±.009±.020	.342
91.0	.644±.015±.057	.668		89.3	.333±.015±.031	.346
111.7	.659±.029±.058	.664		110.3	.314±.022±.034	.324
124.8	.665±.020±.037	.661		126.5	.341±.017±.032	.318
141.2	.695±.026±.043	.688		150.0	.339±.015±.022	.351
157.4	.680±.018±.033	.668		174.4	.321±.015±.021	.354
165.1	.714±.020±.035	.666		201.9	.303±.017±.026	.340
179.8	.727±.015±.036	.680				
190.8	.749±.015±.035	.694				
212.5	.709±.014±.048	.637				
229.1	.756±.018±.052	.680				
Average	.669±.003±.024				.340±.003±.020	

Table 2

Total cross-section slopes in energy bins with and without the flux smoothing procedure. To avoid repetition, errors are only shown on one set and are statistical first and systematic second (they do not include an overall scale error of 3% for neutrinos and 5.5% for antineutrinos). All cross-section slopes are in units of $10^{-38} \text{cm}^2/\text{GeV}$.

The structure functions resulting from our analysis are shown in table 7 for the assumptions $R = 0.1$ and R_{QCD} (see equation 11). The errors shown in the table are statistical only. Figures 8 and 9 show the results assuming $R = R_{QCD}$.

3 Quark-Parton Model Tests

These results have been compared with predictions of the Quark-Parton model and of QCD [25,26]. The Quark-Parton model relates $F_2^{\mu N}$ obtained from charged lepton scattering to that obtained from neutrino scattering by the mean square charge of the constituent quarks:

$$F_2^{PRED} = \frac{18}{5} F_2^{\mu N} / \left(1 - \frac{3s + \bar{s}}{5q + \bar{q}}\right) \quad (4)$$

taking $c = \bar{c} = 0$. Comparisons of structure functions from various neutrino and muon scattering experiments can therefore be made. For these comparisons it was again assumed

that the strange sea is $1/2$ SU(3) symmetric. The ratio of F_2 from this data to F_2^{PRED} , as calculated from published muon scattering data from iron by the European Muon Collaboration (EMC) [16] is shown in figure 2. The data have been interpolated to $Q^2 = 10\text{GeV}^2/c^2$ in this comparison, and the value of $F_2^{\mu N}$ adjusted to the assumption of $R = 0.1$. The predicted value falls below our measurement by about 10%, but exhibits no x dependence. This is near the combined estimated systematic normalization errors of 3% for EMC and 5% for our result. There has been some evidence that the normalization of the result from EMC is systematically lower than that of other charged lepton scattering experiments [17]. A recent measurement [18] of $F_2^{\mu N}$ from iron is also systematically larger than EMC values by 4.7%. The comparison between neutrino and muon data is not seriously affected by assumptions about the strange sea, either in evaluating F_2^{PRED} or in extracting F_2 from neutrino scattering data. Reasonable changes in assumptions about the strange sea or the charm quark mass do not appreciably change the result. Also included in figure 2 is the corresponding result using F_2 from CDHS [12]. The difference between results obtained for F_2 reported here and CDHS is not simply a level difference as implied by the difference in the total cross sections. Our result for F_2 is more strongly peaked at small x than the data of CDHS.

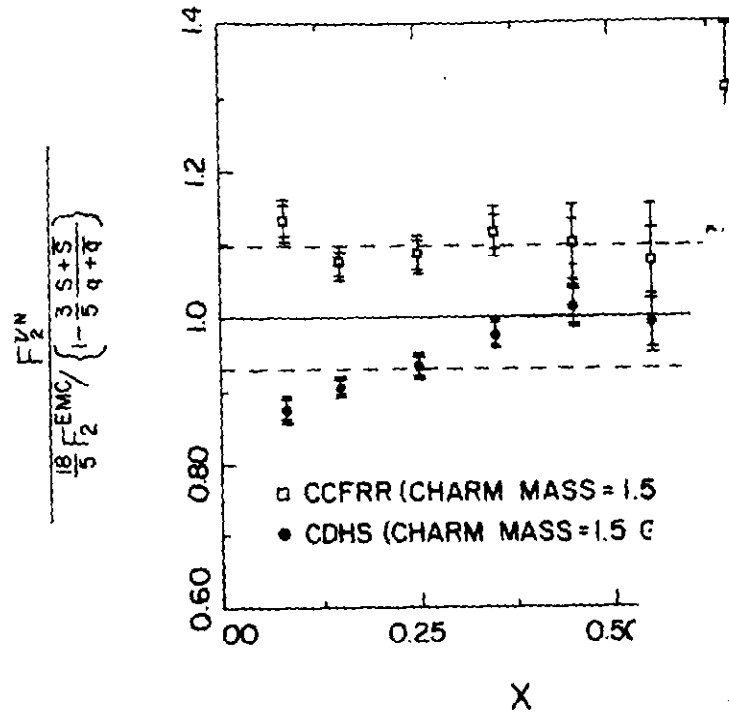


Figure 2

Ratio of F_2 for CCFRR and CDHS to F_2^{EMC} from EMC at $Q^2=10\text{GeV}^2$. The numbers on the right are averages which include overall normalization errors.

Also sensitive to overall levels is the test of the Gross-Llewellyn-Smith (GLS) sum rule:

$$\int_0^1 F_3(x, Q^2) dx = 3 \left(1 - \frac{\alpha_S(Q^2)}{\pi} \right) \quad (5)$$

Equation 5 is the prediction including the $O(\alpha_S)$ correction from QCD beyond the leading log approximation. The experimental result for the GLS sum rule [26] is strongly influenced by the determination of $x F_3$ at low x . Roughly half of the integral over F_3 comes from the region below $x = 0.06$. The excellent small x resolution of this experiment allows us to make a nearly model independent measurement. Since the small x region is critical, a result can only be obtained at low Q^2 . Because the values of E_h are high, these data are typically at high W^2 . At $Q^2=3\text{GeV}^2$, we obtain

$$\int_0^1 F_3(x) dx = 2.83 \pm .15 \pm .09 \pm .10$$

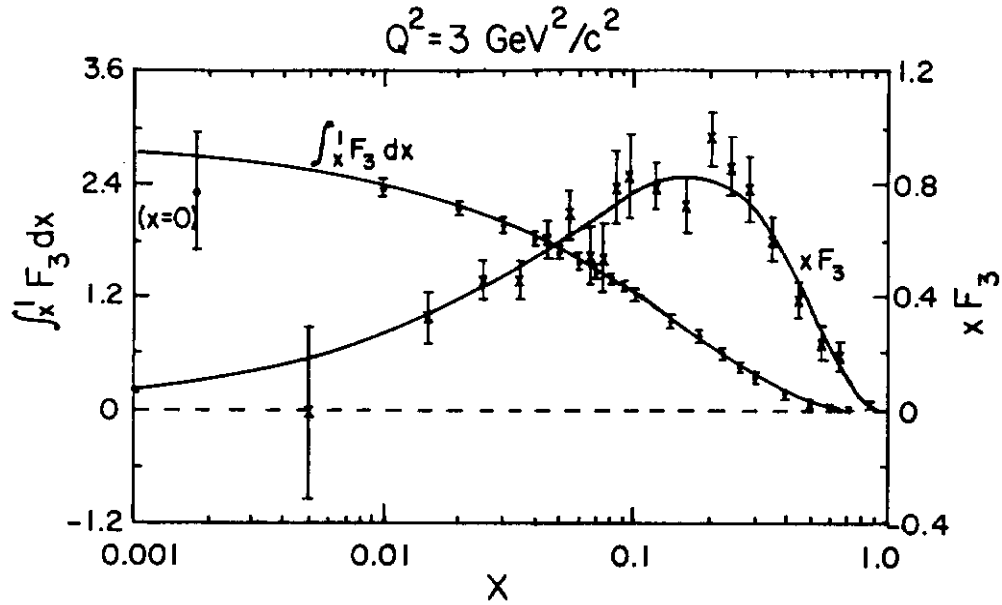


Figure 9

xF_3 in fine x bins at $Q^2 = 3 \text{ GeV}^2$ with the fit (8). Also shown is $\int_x^1 F_3 dx$ from the fit with points from the simple summation technique superimposed. The right scale (crosses) is xF_3 at $Q^2 = 3 \text{ GeV}^2$. The left scale (diamonds) corresponds to $\int_x^1 F_3 dx$ at $Q^2 = 3 \text{ GeV}^2$. In the most important region $x < .06$, W^2 is always larger than 16.5 GeV^2 .

where the first error is statistical, the second comes from correlated ν and $\bar{\nu}$ flux errors and the third accounts for other systematic errors. Fine bins were made at low x and in every bin the data has been interpolated to a fixed Q^2 . The integral of F_3 above $x = 0.01$ is virtually independent of the integration technique used, including direct summation of xF_3/x . The error for the $x < 0.01$ region is dominated by the error in the exponent of x in fits of the form Ax^{b_3} . A fit using the region $x < .06$ gives $b_3 = 0.58 \pm .18$, whereas a global fit ($0 < x < 1$) using the form in (8) gives $b_3 = 0.58 \pm .06$. The expectation [19] that xF_3 behaves like \sqrt{x} at small x is also satisfied. The global QCD fit in section 4 gives $2.70 \pm .15$ for the value of $\int_0^1 F_3 dx$ at $Q_0^2 = 12.6 \text{ GeV}^2$. All of these values are consistent with QCD expectations for $\Lambda_{LO} < 525 \text{ MeV}$ using statistical errors. Figure 3 shows the variation in xF_3 as a function of x (on a log scale). The integrated value of F_3 is also shown. The consistency with \sqrt{x} at small values of x is obvious.

4 QCD Formalism

QCD predicts logarithmic scaling violations in the structure functions due to quark bremsstrahlung and gluon pair production processes which increase with decreasing distance over which the nucleon is probed. This effect is described by the Altarelli-Parisi equations [20] which allow the calculation of the value of the structure functions at some evolved Q^2 , given the structure function at some Q_0^2 . In leading order:

$$\begin{aligned}\frac{dF_2(x, Q^2)}{d \ln Q^2} &= \frac{\alpha_S(Q^2)}{2\pi} \{P_{qq}(x) \otimes F_2(x, Q^2) + 2N_f P_{gq}(x) \otimes G(x, Q^2)\} \\ \frac{dG(x, Q^2)}{d \ln Q^2} &= \frac{\alpha_S(Q^2)}{2\pi} \{P_{gg}(x) \otimes F_2(x, Q^2) + P_{gq}(x) \otimes G(x, Q^2)\} \\ \frac{dx F_3(x, Q^2)}{d \ln Q^2} &= \frac{\alpha_S(Q^2)}{2\pi} \{P_{qq}(x) \otimes x F_3(x, Q^2)\}\end{aligned}\quad (6)$$

where the terms in brackets are of the general form:

$$f(x) \otimes g(x) = \int_x^1 f(z) g\left(\frac{x}{z}\right) \frac{dz}{z}$$

The P_{ij} are splitting functions given by QCD, and $G(x, Q^2)$ is the gluon distribution of the nucleon. The strong coupling constant is, to leading order,

$$\alpha_S(Q^2) = \frac{12\pi}{(33 - 2N_f) \ln Q^2 / \Lambda_{LO}^2} \quad (7)$$

where the scale parameter Λ_{LO} is to be experimentally determined. The number of quark flavors, N_f , was taken to be four.

The procedure used to determine Λ is to parameterize F_2 , G and $x F_3$ at some Q_0^2 :

$$\begin{aligned}F_2(x, Q_0^2) &= a_2(1-x)^{c_2}(1 + \gamma_2 x) \\ x F_3(x, Q_0^2) &= a_3 x^{b_3} (1-x)^{c_3} \\ G(x, Q_0^2) &= a_G(1-x)^{c_G}(1 + \gamma_G x)\end{aligned}\quad (8)$$

and then to use the evolution equations to compute the predicted value at any other Q^2 . Separate least square fits to F_2 and $x F_3$ are used to extract the various unknown parameters and Λ . Target mass corrections are very small in the regions of x and Q^2 studied and are applied using the prescription of Georgi and Politzer [21] for the F_2 analysis. For the purposes of the $x F_3$ analysis we have verified that these corrections are small (<3% change in α_S) in the regions studied.

5 F_2 Analysis

The structure function F_2 is proportional to the sum of neutrino and anti-neutrino differential cross sections, and therefore has small fractional statistical errors. However the Q^2 evolution of F_2 is complicated by the coupling to the unknown gluon distribution G . In addition, extraction of this structure function is sensitive to assumptions about R and the strange sea. Fits are made to the data in the region $Q^2 > 5\text{GeV}^2$ and $W^2 > 10\text{GeV}^2$ where corrections from the finite target mass, higher twist and quark mass thresholds are small. We use a computer program obtained from D. Duke and J. Owens and described in reference 23 for both first and second order fits. Data below $x = 0.1$ are eliminated to limit reliance on uncertain assumptions about the strange sea. The normalization of the gluon distribution at $Q_0^2 = 5\text{GeV}^2$ is constrained by the momentum sum rule:

$$\int_0^1 G(x, Q^2) dx = 1 - \int_0^1 F_2(x, Q^2) dx \quad (9)$$

A QCD fit using the F_2 values from this experiment (table 7) with fixed reasonable gluon parameters ($c_G = 4.6$ and $\gamma_G = 9.0$), yielded the parameters listed in table 3. The second order fit, made using the method of reference 23, is shown in the last column of the table. The fit is slightly worse than the leading order fit and the value of A is slightly larger.

	Leading Order	Second Order($\overline{\text{MS}}$)
Λ	$360 \pm 100\text{MeV}$	$340 \pm 110\text{MeV}$
c_2	$2.85 \pm .16$	$3.36 \pm .15$
a_2	$1.525 \pm .086$	$1.808 \pm .092$
γ_2	$1.87 \pm .56$	$2.14 \pm .57$
χ^2	45.5 for 39 DF	45.5 for 39 DF

	Λ_{LO}	$\Lambda_{\overline{\text{MS}}}$
$R = 0.0$	$360 \pm 100\text{MeV}$	$390 \pm 110\text{MeV}$
$R = 0.1$	$200 \pm 90\text{MeV}$	$230 \pm 100\text{MeV}$
R_{QCD}	$300 \pm 100\text{MeV}$	$340 \pm 110\text{MeV}$

Table 9 F_2 fits with $c_G = 4.6$, $\gamma_G = 9.0$ and $R = 0.1$

In leading order QCD, R is expected to be zero. To second order, the longitudinal structure function $F_L (=2xF_1R)$ is given by

$$F_L = \frac{\alpha_S(Q^2)}{2\pi} x^2 \int_x^1 \frac{dy}{y^3} \left\{ \frac{8}{3} F_2(y, Q^2) + 4n_f \left(1 - \frac{x}{y}\right) y G(y, Q^2) \right\} \quad (10)$$

This implies that R is small at large x , large at small x and decreases logarithmically with increasing Q^2 . Using a modified version of our F_2 evolution program we have parameterized the dependence of R on F_2 and G by the form

$$R = \frac{.73(1-x)^{3.7}}{\ln(Q^2/.24^2)} \quad (11)$$

Values for Λ have been extracted using R_{QCD} and the assumptions $R=0$ and $R=0.1$. They are also listed in table 3 and all lie within 160 MeV of each other.

It is well known [22,23] that the fitted value of Λ is strongly correlated with the parameters characterizing the gluon distribution. Fits using F_2 alone are unable to significantly constrain these gluon parameters. The Quark-Parton model and asymptotic QCD [24] predict that the gluon distribution behaves at large x like $(1-x)^{c_3+1}$. As reported below fits to xF_3 show that $c_3 \approx 3.4$. It is reasonable to expect that the gluon parameters lie within the limits: $4 \leq c_G \leq 8$ and $\gamma_G \geq 0$. The correlation between the best value for Λ_{LO} and c_G for various values of γ_G is shown in figure 4. The rms contribution to the determination of Λ is found to be about $\pm 50\text{MeV}$, if all values of the gluon parameters within the noted limits are equally probable.

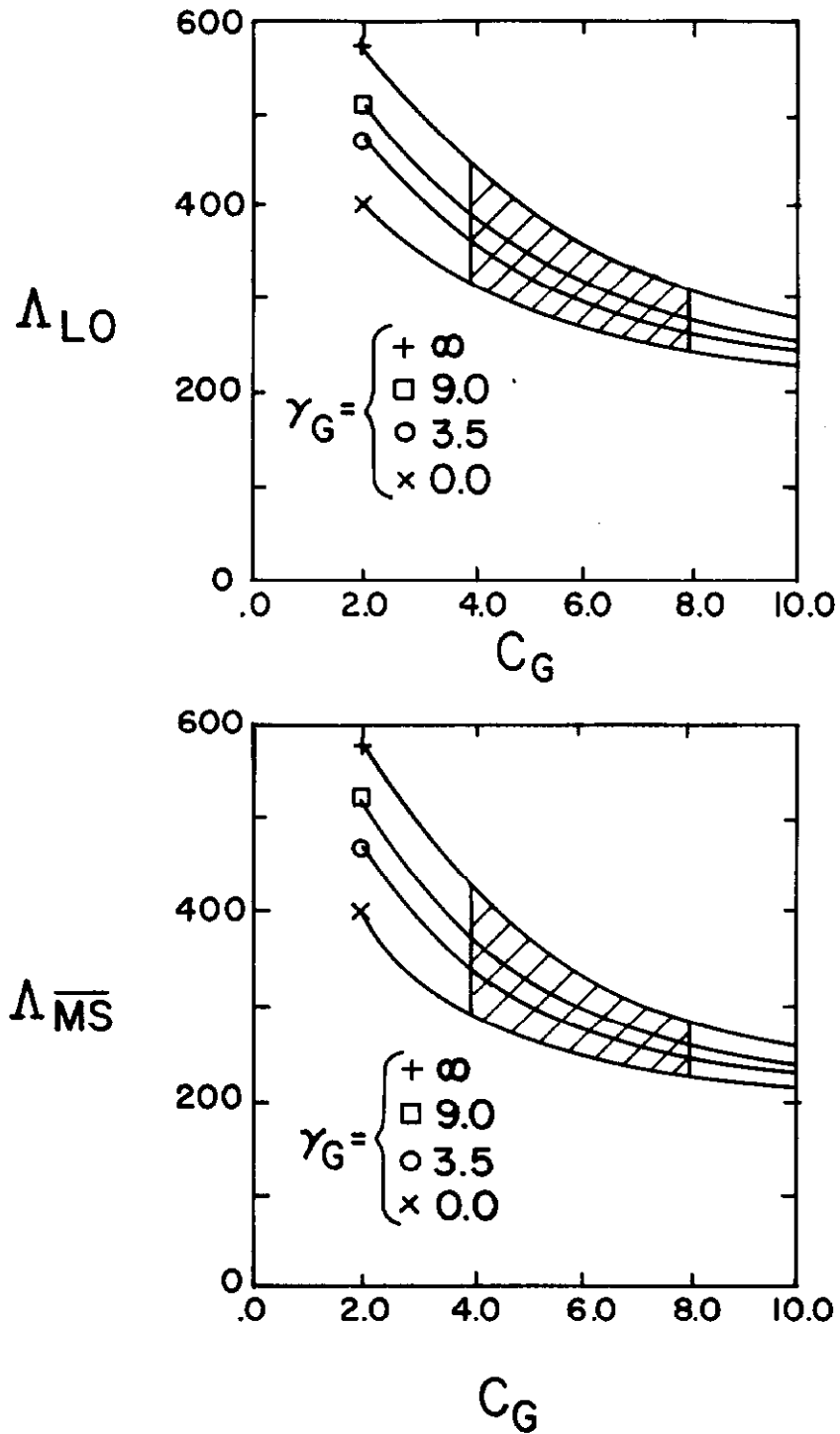


Figure 4 Correlation between best values for Λ from F_2 and gluon parameters

Table 4 shows changes in Λ_{LO} for variation of several assumptions made in fitting F_2 . The single largest source of uncertainty in Λ_{LO} arises from assumptions about the gluon distribution. The strange sea uncertainty contributes the next largest error. The errors due to uncertainties in the setting to setting ν and $\bar{\nu}$ fluxes from our smoothing technique and those from overall level uncertainties are also shown.

Source	Change in Λ_{LO}
Gluon distribution	± 50 MeV
Strange sea	± 35 MeV
Flux smoothing	± 25 MeV
Flux level	± 30 MeV
Secondary beam dispersion	± 10 MeV
Hadron energy calibration	± 15 MeV
Muon energy calibration	± 15 MeV
Total, excluding gluon dist.	± 57 MeV

Table 4 Estimated systematic errors on Λ_{LO} from fits to F_2

6 xF_3 Analysis

The structure function xF_3 measured in deep inelastic neutrino scattering is unique in that the extracted value of this structure function is almost independent of the value of R , and its QCD evolution does not depend on the gluon density. However, since xF_3 is essentially the difference of the ν and $\bar{\nu}$ differential cross-sections, it has larger fractional statistical errors than F_2 .

Two different computer programs have been used to evolve xF_3 to both first and second order [20]: one was obtained from R.M. Barnett [22] and the previously mentioned one from D. Duke and J. Owens [23]. The programs solve the differential equation (6) to first and second order starting at $Q_0^2 (=12.6 \text{ GeV}^2)$ with the parameterization of $xF_3(x, Q_0^2)$ shown in equations (8). The GLS sum rule (5) is not used to constrain the normalization since the very small x region is not being used in these fits. The constants a_3 , b_3 and c_3 are determined as parameters along with Λ . Cuts are imposed to eliminate regions where non-perturbative QCD effects may be significant. These are:

$$Q^2 > 5\text{GeV}^2, \quad W^2 > 10\text{GeV}^2, \quad .04 < x < .7$$

It should be noted that the two programs agree well in leading order. At the 90% CL

we find that $\Lambda_{LO} < 420$ MeV. The best fit parameters are

$$\begin{aligned}
 \Lambda_{LO} &= 88_{-78}^{+163} \text{ MeV} \\
 \alpha_S &= .204 \pm .079 \text{ for } Q_0^2 = 12.6 \text{ GeV}^2 \\
 b_3 &= .672 \pm .058 \\
 c_3 &= 3.29 \pm .24 \\
 a_3 &= 4.34 \pm .24 \\
 \chi^2 &= 44.2 \text{ for 45 DF}
 \end{aligned} \tag{12}$$

The curve labelled " xF_3 " in figure 5 shows the χ^2 versus Λ for this fit. Note that, this best value for Λ_{LO} from xF_3 , together with the results from F_2 shown in figure 4, indicate that larger values of c_G i.e., "softer" gluon distributions, are preferred. This is a weak conclusion at present, because of the limited statistical precision of the data.

The same non-singlet analysis has been performed by the standard technique [23] of combining experimental values of xF_3 below $x = 0.4$ and F_2 above $x = 0.4$. This implicitly assumes a vanishing sea and small R in the high- x region, or equivalently that $xF_3 = F_2$ above $x = 0.4$. The resulting parameters agree with those above:

$$\begin{aligned}
 \Lambda_{LO} &= 266_{-104}^{+114} \text{ MeV} \\
 \alpha_S &= .291 \pm .047 \text{ for } Q_0^2 = 12.6 \text{ GeV}^2 \\
 b_3 &= .635 \pm .049 \\
 c_3 &= 2.90 \pm .13 \\
 a_3 &= 4.29 \pm .22 \\
 \chi^2 &= 50.0 \text{ for 46 DF}
 \end{aligned}$$

The curve labelled " xF_3/F_2 " in figure 5 shows the χ^2 versus Λ for this fit. The substantial reduction in errors is quite clear in the figure.

The non-linear nature of the dependence of the evolution equations (6) on Λ , combined with large statistical errors on xF_3 , results in the asymmetric shape of the curves in figure 5. The dependence of χ^2 on $\alpha_S(Q_0^2 = 12.6 \text{ GeV}^2)$ is shown in figure 6. Because of the more linear dependence on α_S in (6), these curves are much more symmetric. For this reason, in the investigation of changes due to several systematic effects below, we look at the behaviour of $\alpha_S(Q_0^2 = 12.6 \text{ GeV}^2)$ instead of the behaviour of Λ . It should be noted that from either fit, the hypothesis that $\alpha_S = 0$ or $\Lambda = 0$ is poor ($\chi^2 = 52.7$, 46 d.f. for xF_3 alone; $\chi^2 = 100.6$, 47 d.f. for " xF_3/F_2 "). In both cases, the χ^2 at the best fit is acceptable using statistical errors only.

Possible correlations among the parameters were determined from the fit to xF_3 alone. $\alpha_S(Q_0^2)$ has virtually no correlation with $\int F_3 dx$ and with b_3 . The correlation with c_3 however, is strong, and is shown in figure 7. This indicates that the high- x dependence of xF_3 affects the value of Λ to some extent.

The parameters in (12) imply $\int F_3 dx = 2.70 \pm .15$ as quoted in section 4. This value is consistent with the result of the GLS sum rule analysis. It should be noted that this fit does not utilize the very low- x data. The reduced statistical error is related to the additional constraints imposed by the specific parameterization, equation (8).

The effects of changing the forms of the fitting functions were not found significant; for example, increasing the number of parameters in the fit by the inclusion of a $(1 + \gamma x)$ term does not change Λ significantly. Λ is also unaffected by varying the Q_0^2 at which $x F_3$ is parameterized and by iterating the structure function extraction. Columns 2 and 3 of table 5 show the changes in $\alpha_S(Q_0^2)$ resulting from these and several other changes in the assumptions made in extracting structure function values and using them in the two fits described above. The last four items give the effect of changing the number of flavors, including the $(1 + \gamma x)$ term, changing Q_0^2 and changing assumptions about the strange sea. These have very little effect on $\alpha_S(Q_0^2)$.

The first two items in the table, which produce larger changes in α_S , require some comment. As mentioned previously, the data used here were obtained at several different beam energy settings. The resulting cross-section slopes are consistent, within expected fluctuations, with being independent of energy as well as with the small dependence on energy calculated from integrating the QCD parameterization. Since any quark-parton model would give a smooth dependence on energy, the data were constrained to satisfy this hypothesis. This was done by requiring that the number of events at a given energy setting agree with a prediction from integrals of the averaged structure functions. The changes in α_S tabulated in the first row result from the variations within the errors of our cross-section smoothing procedures. The value of $x F_3$, since it comes from the difference in neutrino and anti-neutrino data, is sensitive to the uncorrelated normalization errors in the cross-section measurements. The numbers in the second row reflect the changes in $\alpha_S(Q_0^2)$ calculated due to these errors. Although these effects are smaller than the statistical error on α_S , it is clear that precise measurements of Λ with this technique require high precision on normalized cross-sections.

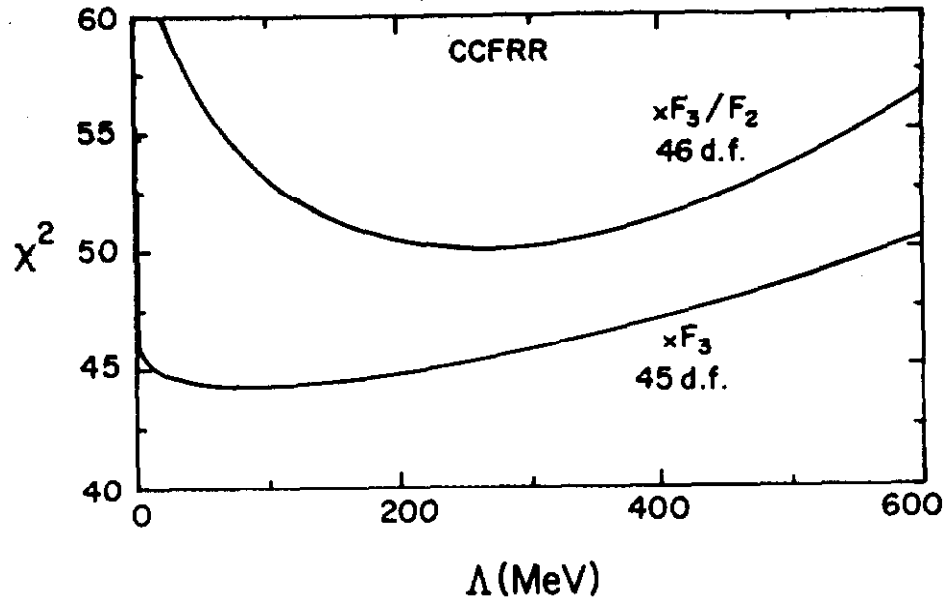


Figure 5 χ^2 versus Λ_{LO} for fits to xF_3 and " xF_3/F_2 "

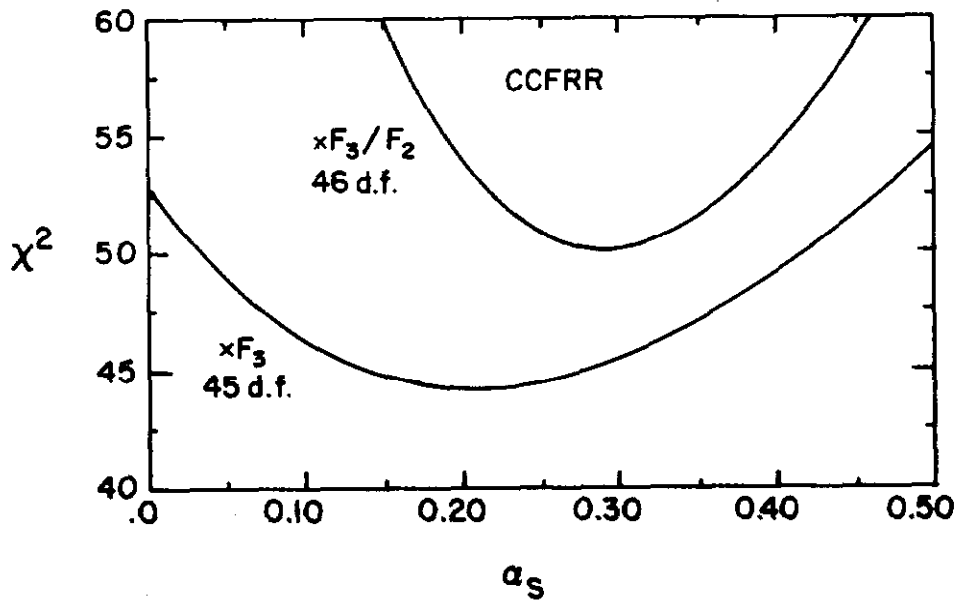


Figure 6 χ^2 versus α_S for fits to xF_3 and " xF_3/F_2 "

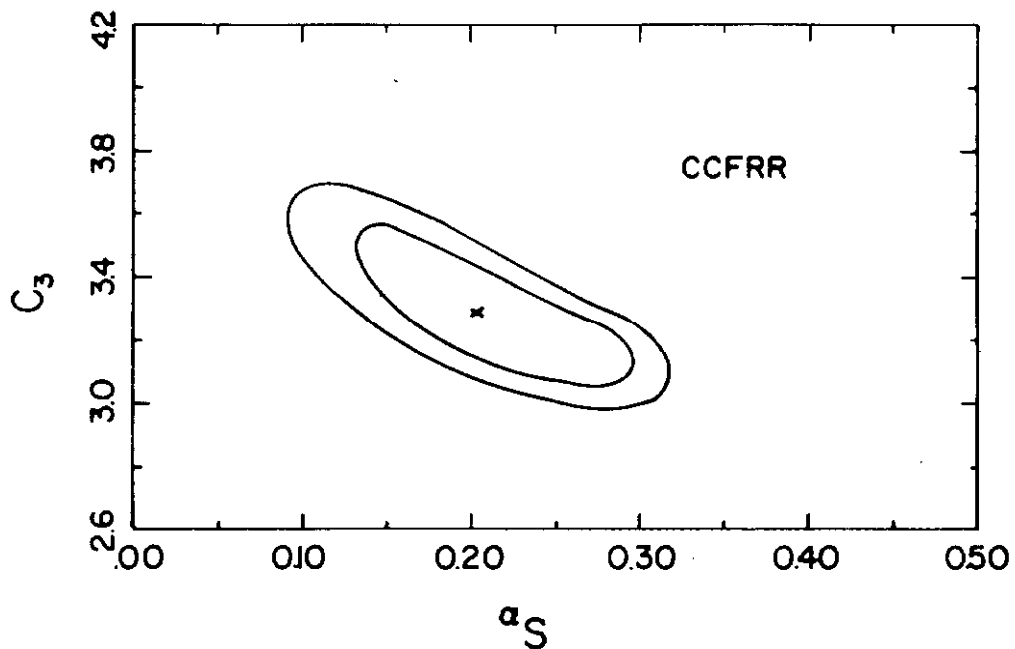


Figure 7

Correlation between α_S and c_3 used in fitting xF_3 . Shown are one and two standard deviation contours.

The sensitivity of the alternative method, which used F_2 values at large x , is also shown in table 5. The different sensitivity with this method reflects both the different way F_2 depends on the assumptions and the different statistical precision of this data. In all cases, these changes in α_S (or Λ) are smaller than the statistical errors of 0.079 for the xF_3 fit and 0.047 for the " xF_3/F_2 " fit. It should be noted that the first two systematic errors which come from flux uncertainties, while valid for this experiment, are partially limited by statistics and should be smaller for a higher statistics experiment.

Systematic effect	xF_3	" xF_3/F_2 "
Cross-section smoothing	.027	.010
Cross-section level errors	.047	.006
$n_f = 4$ changed to $n_f = 3$.001	.003
Inclusion of γ_x term	.0003	.002
Change in Q_0^2 (12.6 GeV ²)	.001	.001
1/2 SU(3) changed to SU(3)	.002	.002
Different R assumptions	.004	.015
Different models for correction terms in F_2 , xF_3 extraction	.008	.006
Systematic error in E_{HAD}	.011	.011
Systematic error in E_μ	.014	.009
Beam angular dispersion error	.019	.024

Table 5 Estimated effect on α_S due to changes in assumptions.

Finally, we remark on several attempts to fit the data using prescriptions for second-order QCD. These should each give $\Lambda_{\overline{MS}}$, the scale parameter in the modified minimal subtraction scheme, which should minimize the differences from Λ_{LO} . In contrast to the agreement among the leading-order fits, we find some differences between the second order fits using the two available computer programs [22,23]. Table 6 shows the values of Λ and α_S , with statistical errors, resulting from these fits.

There are technical differences among the programs. That of D. Duke and J. Owens [23] uses a definition of parton densities that makes them "universal", the same densities applicable in any process. Structure functions are constructed from evolved parton densities. The other technique [22] is one in which certain cross section terms are absorbed into the definition of parton densities and the structure functions are evolved directly [24]. In principle, both programs should give the same value for $\Lambda_{\overline{MS}}$ if the true expression (or functional form) for xF_3 and the parton density were known at $Q^2 = Q_0^2$ and if all non-perturbative effects were absent. However, since these expressions are unknown, both the computer programs utilize the *same* parameterization for these *different* distributions and therefore lead to the different values for $\Lambda_{\overline{MS}}$. It should be noted that the change in $\alpha_S(Q_0^2)$ in going from leading to second order is not large.

Method	Λ (MeV)	$\alpha_S(Q^2 = 12.6 GeV^2)$
Leading Order	88^{+183}_{-78}	$.204 \pm .079$
\overline{MS} Barnett (ref. 22)	120^{+200}_{-106}	$.176 \pm .062$
\overline{MS} Duke(ref. 23)	193^{+272}_{-158}	$.201 \pm .070$

Table 6 Λ and α_S resulting from first and second(\overline{MS}) order fits

7 Conclusions

The high statistics neutrino-nucleon scattering data from the Fermilab experiment E616 have been used to extract the F_2 and xF_3 structure function data shown in table 7. From this data, it is concluded:

(1) The Quark-Parton model comparison of $F_2(x)$ with the analogous structure function measured in muon scattering by the EMC group [16] shows a level difference of about 10%, possibly due to systematic normalization differences among experiments. The x -dependence of the two structure functions is very similar. This comparison indicates agreement with the mean squared quark charge prediction at the 10% level.

(2) Measurement of the GLS sum rule gives

$$\int_0^1 F_3 dx = 2.83 \pm .20$$

consistent with the Quark-Parton model and QCD with $\Lambda < 525$ MeV.

(3) Fits to F_2 in leading order and second order give, with statistical errors,

$$\begin{aligned} \Lambda_{LO}^{F_2} &= 360 \pm 100 \text{ MeV} \\ \Lambda_{\overline{MS}}^{F_2} &= 340 \pm 110 \text{ MeV} \end{aligned}$$

for a particular choice of gluon distribution. Variations of the parameters in the gluon distribution over reasonable limits indicate an additional rms uncertainty of approximately 50MeV. Other systematic uncertainties, such as R and flux uncertainties, indicate a net systematic error comparable to the statistical error.

(4) A fit to xF_3 in leading order gives, with statistical error,

$$\Lambda_{LO}^{xF_3} = 88^{+183}_{-78} \text{ MeV}$$

A fit assuming $R = 0$ and $\bar{q} = 0$ for $x > 0.4$, so that the better determined F_2 may be used at large x , gives

$$\Lambda_{LO}^{xF_3/F_2} = 266^{+114}_{-104} \text{ MeV}$$

The systematic errors (table 5) are clearly smaller than the statistical errors for the two fits.

(5) Second order fits [22,23] to xF_3 give somewhat different values of Λ , although the values of $\alpha_S(Q_0^2 = 12.6 \text{ GeV}^2)$ are not so strikingly different (table 6).

Table 7

x	Q^2	F_2 (R=0.1)	F_2 R_{QCD}	ΔF_2 R_{QCD}	$x F_3$ (R=0.1)	$x F_3$ R_{QCD}	$\Delta x F_3$ R_{QCD}
.015	1.26	1.256	1.287	.051	.171	.165	.058
	2.00	1.308	1.343	.058	.376	.366	.056
	3.16	1.499	1.537	.084	.309	.303	.076
	5.01	1.370	1.402	.116	.434	.431	.106
	7.94	1.548	1.584	.269	-	-	-
.045	1.26	1.134	1.134	.050	.448	.440	.143
	2.00	1.350	1.359	.047	.627	.620	.089
	3.16	1.348	1.363	.044	.615	.608	.062
	5.01	1.528	1.545	.059	.513	.508	.072
	7.94	1.647	1.662	.081	.696	.693	.094
	12.59	1.520	1.531	.113	.647	.646	.116
	19.95	1.068	1.071	.197	.630	.631	.182
.080	1.26	1.247	1.244	.128	-	-	-
	2.00	1.447	1.445	.055	.620	.615	.182
	3.16	1.486	1.487	.046	.774	.769	.103
	5.01	1.460	1.464	.044	.668	.666	.070
	7.94	1.542	1.545	.051	.657	.655	.069
	12.59	1.592	1.591	.068	.781	.781	.085
	19.95	1.584	1.576	.090	.771	.771	.098
	31.62	1.241	1.228	.166	.662	.662	.162
.150	2.00	1.194	1.183	.109	-	-	-
	3.16	1.186	1.180	.036	.733	.732	.135
	5.01	1.284	1.280	.028	.689	.689	.073
	7.94	1.241	1.235	.025	.878	.878	.046
	12.59	1.242	1.232	.028	.854	.855	.042
	19.95	1.305	1.292	.036	.789	.790	.049
	31.62	1.290	1.270	.046	.846	.847	.055
	50.12	1.188	1.161	.075	.799	.799	.080
	79.43	0.917	0.889	.251	.705	.704	.239
.250	3.16	1.874	1.868	.724	-	-	-
	5.01	1.028	1.026	.039	.622	.623	.161
	7.94	0.989	0.985	.026	.792	.794	.076
	12.59	0.941	0.933	.024	.794	.797	.048
	19.95	0.936	0.923	.026	.766	.770	.042
	31.62	0.968	0.952	.033	.795	.799	.050
	50.12	0.862	0.840	.034	.745	.747	.042
	79.43	0.777	0.747	.053	.649	.650	.057
125.89	0.598	0.568	.279	-	-	-	

x	Q^2	F_2 ($R=0.1$)	F_2 R_{QCD}	ΔF_2 R_{QCD}	xF_3 ($R=0.1$)	xF_3 R_{QCD}	ΔxF_3 R_{QCD}
.350	5.01	0.882	0.882	.189	-	-	-
	7.94	0.677	0.676	.027	.581	.584	.108
	12.59	0.652	0.649	.023	.550	.553	.060
	19.95	0.645	0.638	.024	.466	.469	.047
	31.62	0.637	0.627	.027	.509	.512	.048
	50.12	0.600	0.587	.028	.559	.563	.041
	79.43	0.619	0.597	.037	.499	.500	.045
	125.89	0.719	0.684	.076	.266	.266	.083
.450	7.94	0.498	0.498	.041	-	-	-
	12.59	0.421	0.419	.020	.450	.452	.068
	19.95	0.398	0.395	.019	.304	.306	.043
	31.62	0.388	0.382	.020	.317	.319	.038
	50.12	0.354	0.347	.021	.337	.340	.036
	79.43	0.385	0.375	.026	.315	.317	.037
	125.89	0.292	0.279	.028	.303	.303	.032
	199.53	0.307	0.290	.132	.300	.302	.139
.550	12.59	0.241	0.241	.017	.217	.218	.071
	19.95	0.232	0.231	.015	.167	.168	.044
	31.62	0.209	0.206	.014	.207	.209	.029
	50.12	0.202	0.198	.018	.170	.171	.033
	79.43	0.203	0.199	.020	.167	.169	.031
	125.89	0.156	0.150	.019	.169	.170	.024
	199.53	0.128	0.120	.040	.130	.130	.044
.650	12.59	0.150	0.150	.018	.161	.163	.080
	19.95	0.121	0.120	.010	.170	.171	.033
	31.62	0.139	0.138	.015	.121	.122	.039
	50.12	0.112	0.111	.015	.071	.072	.030
	79.43	0.100	0.098	.016	.058	.058	.028
	125.89	0.095	0.092	.014	.098	.099	.018
	199.53	0.071	0.068	.020	.076	.076	.023

Table 7 $F_2(x, Q^2)$ and $xF_3(x, Q^2)$ for R_{QCD} and $R = 0.1$ (statistical errors only).

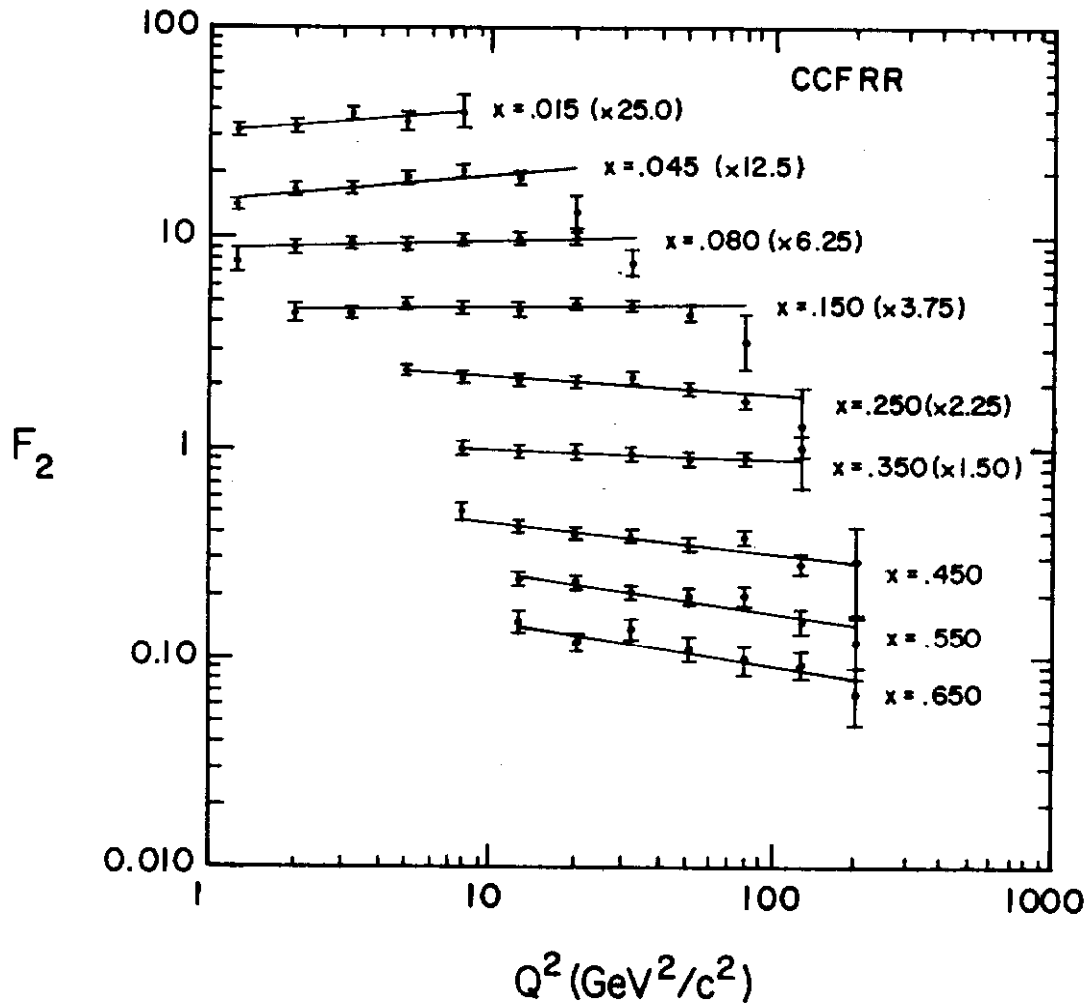


Figure 8 $F_2(x, Q^2)$ assuming $R=R_{QCD}$ (see text).
The solid lines are linear fits in $\log Q^2$.

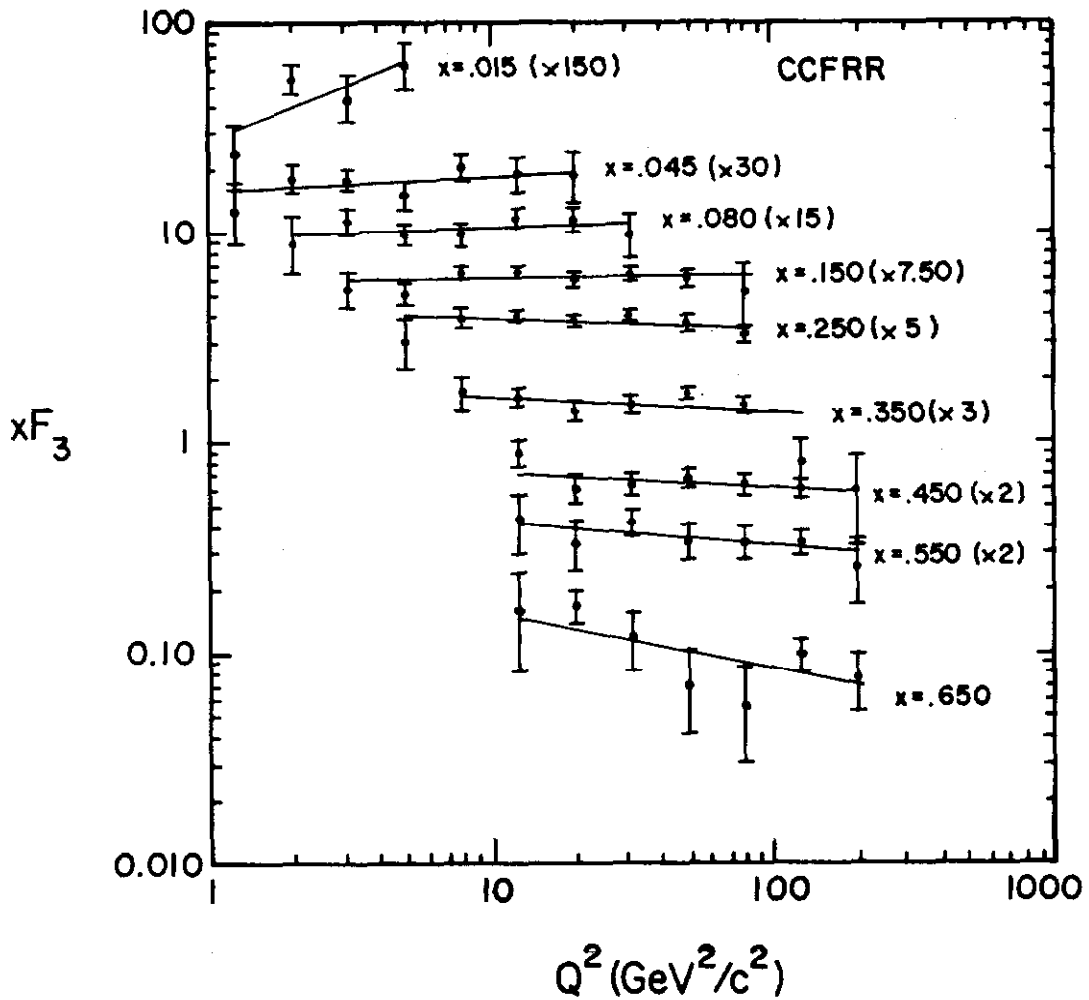


Figure 9 $x F_3(x, Q^2)$ assuming $R=R_{QCD}$ (see text).

The solid lines are linear fits in $\log Q^2$.

References

- 1 R. Blair et al.: Phys. Rev. Lett, 51, 343 (1983).
- 2 D.A. Edwards and F.J. Sciulli: *A Second Generation Narrow Band Beam*. Fermilab TM-660 (unpublished).
- 3 R. Blair et al.: *A Monitoring and Calibration System for Neutrino Flux Measurement in a High Energy Dichromatic Neutrino Beam*, Nevis Preprint (1983), Fermilab-Pub-83/26-Exp. Submitted to Nucl. Instr. & Methods.
- 4 A. Bodek et al.: Z. Phys. C - Particles and Fields, 18, 289, (1983).
- 5 B.C. Barish et al.: IEEE Trans. on Nucl. Sci., NS-25, 532, (1978).
- 6 J. Lee: *Measurements of $\nu_{\mu}N$ Charged Current Cross Sections from $E_{\nu} = 25\text{ GeV}$ to $E_{\nu} = 260\text{ GeV}$* , Ph.D. Thesis (1980), Caltech, Pasadena, CA.
- 7 R. Blair: *A Total Cross Section and Y Distribution Measurement for Muon Type Neutrinos and Antineutrinos on Iron*, Ph.D. Thesis (1982), Caltech, Pasadena, CA.
- 8 H. Abramowicz et al.: Phys. Lett., 107B, 141 (1981).
- 9 A. de Rújula, R. Petronzio and A. Savoy-Navarro: Nucl. Phys., B154, 394 (1979).
- 10 CCFRR collaboration. Paper in preparation.
- 11 J.G.H. de Groot et al.: Z. Phys. C - Particles and Fields, 1, 143, (1979).
- 12 H. Abramowicz et al.: Z. Phys. C - Particles and Fields, 17, 283 (1983).
- 13 F. Bergsma et al.: Phys. Lett., 123B, 269 (1983).
- 14 J.K. Panman: Ph. D. Thesis, University of Amsterdam (1981).
- 15 S.M. Heagy et al.: Phys. Rev., D23, 1045 (1981).
- 16 J.J. Aubert et al.: Phys. Lett., 105B, 322, (1981).
- 17 H.E. Fisk and F. Sciulli: Ann. Rev. Nucl. &Part. Sci., 32, 499 (1982).
- 18 A.R. Clark et al.: *Measurement of the Nucleon Structure Function in Iron Using 215 and 99 GeV Muons*, LBL-16286 (1983). Submitted to 1983 Lepton-Photon Conference.
- 19 E. Reya: Phys. Reports, 69, 195 (1981).
- 20 G. Altarelli and G. Parisi: Nucl. Phys., B126, 298 (1979).
- 21 H. Georgi and D. Politzer: Phys. Rev., D14, 1829 (1976).
J. Kaplan and F. Martin: Nucl. Phys., B115, 333 (1976).

-
- 22 L.F. Abbott and R.M. Barnett: *Annals Phys*, **125**, 276 (1980).
- 23 A. Devoto, D.W. Duke, J.F. Owens and R.G. Roberts: *Phys. Rev.*, **D27**, 508 (1979).
- 24 G. Altarelli: *Phys. Rep.*, **81**, 1 (1982).
- 25 D.B. MacFarlane: *Nucleon Structure from Neutrino Interactions in an Iron Target with a Study of the Singlet Quark Distribution*, Ph.D. Thesis (1984), Caltech, Pasadena, CA.
- 26 M.V. Purohit: *Nucleon Structure Functions from ν_μ -Fe Interactions and a Study of the Valence Quark Distribution*, Ph.D. Thesis (1984), Caltech, Pasadena, CA.